J. Fluid Mech. (2001), *vol.* 436, *pp.* 59–84. Printed in the United Kingdom

The return to isotropy of homogeneous turbulence

By KWING-SO CHOI[1] AND JOHN L. LUMLEY[2]

[1]School of Mechanical, Materials, Manufacturing Engineering and Management, University of Nottingham, University Park, Nottingham NG7 2RD, UK

[2]Sibley School of Mechanical and Aerospace Engineering, Cornell University, Ithaca, New York 14853, USA

(Received 15 September 1999 and in revised form 28 September 2000)

Three types of homogeneous anisotropic turbulence were produced by the plane distortion, axisymmetric expansion and axisymmetric contraction of grid-generated turbulence, and their behaviour in returning to isotropy was experimentally studied using hot-wire anemometry. It was found that the turbulence trajectory after the plane distortion was highly nonlinear, and did not follow Rotta's linear model in returning to isotropy. The turbulence wanted to become axisymmetric even more than it wanted to return to isotropy. In order to show the rate of return to isotropy of homogeneous turbulence, a map of the ratio of the characteristic time scale for the decay of turbulent kinetic energy to that of the return to isotropy was constructed. This demonstrated that the rate of return to isotropy was much lower for turbulence with a greater third invariant of the anisotropy tensor. The invariant technique was then applied to the experimental results to develop a new turbulence model for the return-to-isotropy term in the Reynolds stress equation which satisfied the realizability conditions. The effect of the Reynolds number on the rate of return to isotropy was also investigated and the results incorporated in the proposed model.

1. Introduction

There has been significant development in the field of the second-order modelling of turbulence in the last three decades (Launder, Reece & Rodi 1975; Reynolds 1976; Lumley 1978; Bradshaw, Cebeci & Whitelaw 1981; Launder 1989; Speziale 1991; Hanjalic 1994; Reynolds & Kassinos 1995). In the second-order modelling, a system of statistically averaged equations is closed at the second moment so that all the third-moment terms appearing in the transport equations for second-moment terms, and one auxiliary equation which determines the length scale, must be modelled. Second-order models certainly have an advantage over lower-order models for flows where the transport of second-moment terms, such as the Reynolds stress and heat flux, play important roles. This is because the physics of the transport of second-moment terms can be built into the second-order models. The return-to-isotropy term, which must be modelled in the second-order modelling of turbulence, is responsible for the exchange of turbulent kinetic energy among its components through the interaction of fluctuating velocities and pressure. It is, therefore, important to study the return-to-isotropy term for a better understanding of turbulence, which should lead to a development of better turbulence models.

In 1951, Rotta proposed a celebrated turbulence model for the return-to-isotropy

term assuming a simple relationship between the rate of return to isotropy and the degree of anisotropy of turbulence. It is a linear model in the sense that the rate of return to isotropy is linearly proportional to the degree of anisotropy. Rotta's model has been used in most of the second-order turbulence models, and has been proved to predict many shear flows quite well (Zeman 1975; Launder *et al.* 1975; Reynolds 1976; Lumley & Newman 1977; Lumley 1978; Chung 1978). However, this does not necessarily mean that the return-to-isotropy term has been modelled well by Rotta's model. One can always compensate a flaw, if any, in modelling turbulence by adjusting model constants in the rest of the terms. In fact, there have been claims from experimentalists that Rotta's linear model does not account for the correct energy redistribution among the components in homogeneous shear flows (Champagne, Harris & Corrsin 1970; Hwang 1971; Harris, Graham & Corrsin 1977). There have also been disagreements on the proportionality constant in Rotta's model: different values were used by different models depending on the turbulence structure and the Reynolds number of a particular flow to be modelled (Rotta 1951; Hanjalic & Launder 1972; Launder *et al.* 1975; Zeman 1975; Reynolds 1976).

Lumley & Newman (1977) and Lumley (1978) developed turbulence models for the return to isotropy, which are functions of both the anisotropy of turbulence and the Reynolds number. It seemed that the dispute on Rotta's constant was over after the introduction of these turbulence models. However, the experimental investigation on the return to isotropy of homogeneous anisotropic turbulence by Gence & Mathieu (1980) raised a new question about the rate of return to isotropy when the third invariant of the anisotropy tensor of turbulence was positive. Here, the third invariant of the anisotropy tensor is positive when one component of turbulent kinetic energy is greater than the other two, and it becomes negative when one component of turbulent kinetic energy is less than the other two. They argued, using their experimental evidence, that the homogeneous turbulence with positive third invariant returns to isotropy at much lower rate than that with negative third invariant. As a result, the turbulence models for the return to isotropy proposed by Lumley & Newman (1977) and Lumley (1978) became questionable: they calibrated their models against only the experimental data for axisymmetric turbulence after a contraction (Uberoi 1956, 1957; Mills & Corrsin 1959), in which case third invariant of the anisotropy tensor was negative. Another problem in modelling the return-to-isotropy term is that the intermediate component of turbulent kinetic energy is not always predicted well using Rotta's model, even if the proportionality constant in the model is adjusted (Lumley 1982; Okibane 1979). It seems that these problems are associated with the fundamental question of whether or not the process of the return to isotropy of homogeneous turbulence is linear.

The return to isotropy of homogeneous turbulence following an axisymmetric contraction was first studied by Uberoi (1956, 1957), then by Mills & Corrsin (1959) and Warhaft (1980). Comte-Bellot & Corrsin (1966) conducted an extensive experimental study of it at several Reynolds numbers, where the streamwise turbulence intensity was slightly greater than the other two components. Their results on the asymptotic behaviour of turbulence with vanishing anisotropy were used by Lumley & Newman (1977) and Lumley (1978) in the construction of turbulence models. Anisotropic turbulence after the plane distortion was studied by Tucker (1970) and Gence & Mathieu (1980). Although both tried to produce a similar type of turbulence, their results were quite different. The third invariant of the anisotropy tensor was positive in Gence & Mathieu (1980), while it was negative in Tucker (1979). There have been further more recent experimental studies by Choi (1983), Choi & Lumley (1983), Le

Penven, Gence & Comte-Bellot (1985) and Makita & Minami (1995), who tried to characterize the behaviour of anisotropic turbulence with positive third invariants. Direct numerical simulations (DNS) of homogeneous turbulence were also carried out to study the return to isotropy of anisotropic turbulence (Rogallo 1981; Lee & Reynolds 1985; Lee 1986; Yamamoto 1985; Ikai & Kawamura 1995), although most of these are limited to very low Reynolds numbers.

There is definitely a lack of information on the return to isotropy of homogeneous turbulence. For example, it is not known how the homogeneous anisotropic turbulence returns to isotropy without external forces. Does each component of turbulent kinetic energy decay proportionally with each of the others as Rotta's model predicts? Does the rate of the return to isotropy depend on the type and degree of anisotropy of turbulence or on the Reynolds number? To answer these questions, three types of homogeneous anisotropic turbulence were created by the plane distortion, axisymmetric expansion and axisymmetric contraction of grid turbulence, and their behaviour in returning to isotropy was experimentally studied. The results were used to develop a new turbulence model for the return-to-isotropy term. The effect of the Reynolds number on the rate of return to isotropy was also investigated and the results incorporated in the proposed model.

2. Theory

2.1. *The Reynolds stress equation*

The Reynolds stress equation for homogeneous flows without mean velocity gradients is given (Lumley 1978) by

$$\frac{\partial}{\partial t}\overline{u_i u_j} = \overline{\frac{p}{\rho}(u_{i,j} + u_{j,i})} - 2\nu\,\overline{u_{i,k}u_{j,k}} \tag{1}$$

By adding and subtracting $\frac{2}{3}\bar{\varepsilon}\delta_{ij}$ to the right-hand side of this equation, we obtain

$$\frac{\partial}{\partial t}\overline{u_i u_j} = \left[\overline{\frac{p}{\rho}(u_{i,j} + u_{j,i})} - 2\nu\,\overline{u_{i,k}u_{j,k}} + \tfrac{2}{3}\bar{\varepsilon}\delta_{ij}\right] - \tfrac{2}{3}\bar{\varepsilon}\delta_{ij}, \tag{2}$$

where $\bar{\varepsilon}$ is the dissipation rate, given by

$$\bar{\varepsilon} = \nu\,\overline{u_{i,j}u_{i,j}}. \tag{3}$$

The quantity in the square bracket in equation (2) is a symmetric second-rank tensor with zero trace, which is solely responsible for the return to isotropy of homogeneous anisotropic turbulence through the interaction between fluctuating velocities and pressure. If we set

$$\bar{\varepsilon}\phi_{ij} = -\left[\overline{\frac{p}{\rho}(u_{i,j} + u_{j,i})} - 2\nu\,\overline{u_{i,k}u_{j,k}} + \tfrac{2}{3}\bar{\varepsilon}\delta_{ij}\right] \tag{4}$$

the Reynolds stress equation becomes

$$\frac{\partial}{\partial t}\overline{u_i u_j} = -\bar{\varepsilon}(\phi_{ij} + \tfrac{2}{3}\delta_{ij}), \tag{5}$$

where ϕ_{ij} is a non-dimensional, symmetric second-rank tensor with zero trace, which we call the return-to-isotropy tensor. We will show later how the return-to-isotropy tensor ϕ_{ij} is modelled using the invariant technique (Lumley 1970, 1978).

We introduce the non-dimensional time τ and the anisotropy tensor b_{ij} defined by

$$\mathrm{d}\tau = \frac{\bar{\varepsilon}}{\overline{q^2}}\mathrm{d}t, \tag{6}$$

$$b_{ij} = \frac{\overline{u_i u_j}}{\overline{q^2}} - \frac{\delta_{ij}}{3}, \quad \overline{q^2} = \overline{u_i u_i}. \tag{7}$$

Note that the anisotropy tensor vanishes identically when the turbulence becomes isotropic. Equation (5) can be written in terms of the anisotropy tensor and non-dimensional time as

$$\frac{\mathrm{d}}{\mathrm{d}\tau} b_{ij} = -(\phi_{ij} - 2b_{ij}). \tag{8}$$

2.2. *The invariant technique*

Using the invariant technique (Lumley 1970, 1978), we can derive the most general form of the return-to-isotropy tensor ϕ_{ij} defined in (4). To do this, we assume that ϕ_{ij} is an isotropic, symmetric second-rank tensor function of a symmetric second-rank tensor b_{ij} and the Reynolds number R_l. By an isotropic function, we mean that the functional relationship is isotropic. In other words, any anisotropy of ϕ_{ij} must result entirely from the anisotropy of b_{ij}, although the values of ϕ_{ij} may not be isotropic. We, therefore, assume that there are no body forces acting on the turbulent flow, nor are there solid boundaries within a few turbulent integral scales. The Reynolds number is defined by

$$R_l = \frac{(\overline{q^2})^2}{9\bar{\varepsilon}v}, \tag{9}$$

where the factor of 9 is included so that $\overline{q^2} = 3u^2$ and $\bar{\varepsilon} = u^3/l$. In other words, the Reynolds number R_l is based on the turbulence length scale l and the velocity scale u of energy-containing eddies.

First, we form an invariant $\phi_{ij}A_iB_j$ by choosing two arbitrary vectors A_i and B_j. Then, the invariant $\phi_{ij}A_iB_j$ must be a function of the invariants formed only by the Reynolds number R_l (a scalar), vectors A_i and B_j and the tensor b_{ij}. Remembering that the tensor b_{ij} is symmetric and the invariant $\phi_{ij}A_iB_j$ is bilinear in A_i and B_j, the only possible invariants that can be formed with A_i, B_j and b_{ij} are $b^0_{ij}A_iB_j$, $b^1_{ij}A_iB_j$ and $b^2_{ij}A_iB_j$. This comes from the Cayley–Hamilton theorem (Lumley 1970), where only the 0, 1, and 2 powers of b_{ij} are linearly independent in three dimensions. Therefore, invariant $\phi_{ij}A_iB_j$ can be expressed by

$$\phi_{ij}A_iB_j = \alpha b^0_{ij}A_iB_j + \beta b^1_{ij}A_iB_j + \gamma b^2_{ij}A_iB_j. \tag{10}$$

Since A_i and B_j are arbitrary vectors, we can remove them from the above to obtain

$$\phi_{ij} = \alpha b^0_{ij} + \beta b^1_{ij} + \gamma b^2_{ij}, \tag{11}$$

where α, β, and γ are functions of the Reynolds number R_l and three independent invariants I, II, and III of the anisotropy tensor, given by

$$I = 0, \quad II = -b_{ij}b_{ji}/2, \quad III = b_{ij}b_{jk}b_{ki}/3. \tag{12}$$

Note that the first invariant I is the trace of the anisotropy tensor b_{ij}, therefore it is identically zero. We further use the fact that the tensor ϕ_{ij} is also traceless, to obtain

$$\alpha = \tfrac{2}{3} II\,\gamma. \tag{13}$$

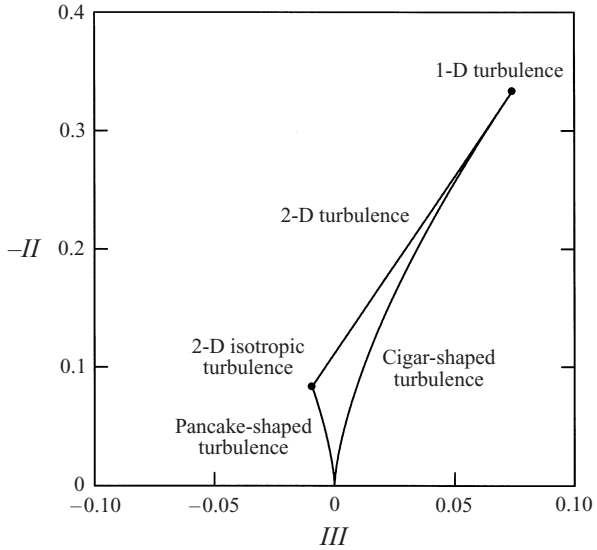

FIGURE 1. The turbulence triangle and possible states of turbulence in invariant coordinates, $-II$ vs. III.

Substituting this relation back into equation (11) we obtain an invariant expression for the return-to-isotropy tensor ϕ_{ij}:

$$\phi_{ij} = \beta b_{ij} + \gamma(b_{ik}b_{kj} + \tfrac{2}{3}II\,\delta_{ij}). \tag{14}$$

This is the most general expression for the return-to-isotropy tensor ϕ_{ij} that is independent of flow geometry and coordinate axes, assuming that there are no suppressed variables other than the Reynolds number R_l and three independent invariants I, II, and III of the anisotropy tensor b_{ij}. Rotta's model (Rotta 1951) assumes that $\gamma = 0$ in equation (14) so it is given by

$$\phi_{ij} = \beta b_{ij}, \tag{15}$$

where β is called Rotta's constant. It will be demonstrated later, however, that the nonlinear term is very important in explaining the nonlinear behaviour in the returning to isotropy of homogeneous anisotropic turbulence.

2.3. *Classification of turbulence*

From equation (7) it can be seen that none of the eigenvalues of the anisotropy tensor b_{ij} can be smaller than $-1/3$, corresponding to the vanishing of turbulent kinetic energy in that component, nor greater than $2/3$, corresponding to the vanishing of other two components (Lumley 1978). This suggests that the range of invariants of the anisotropy tensor is limited by these values. Indeed, it has been demonstrated that all the possible states of turbulence must be found within the turbulence triangle (Lumley & Newman 1977; Lumley 1978) in invariant coordinates as shown in figure 1. The ordinate and the abscissa of this figure are the negative second invariant ($-II$) and the third invariant (III) of the anisotropy tensor, respectively. The two-dimensional (2-D) isotropic state of turbulence, where one component of turbulent kinetic energy vanishes with the remaining two being equal, is at the left-hand corner of the triangle. The one-dimensional (1-D) state of turbulence with only one turbulence component

is at the right-hand corner of the triangle. The origin of the figure corresponds to three-dimensional (3-D) isotropic turbulence. The turbulence along the straight line connecting the 2-D isotropic turbulence and the 1-D turbulence is in the 2-D state. If we define a function F by

$$F = 1 + 27\,III + 9\,II, \tag{16}$$

then F vanishes whenever turbulence becomes two-dimensional, and it becomes unity when turbulence enters a three-dimensional isotropic state. Turbulence on the left-hand side of the triangle is axisymmetric, with one component of the turbulent kinetic energy being smaller than the other two, called pancake-shaped turbulence. Turbulence on the right-hand side of the triangle represents the other type of axisymmetric turbulence, where one component of the turbulent kinetic energy is greater than the other two. This is called cigar-shaped turbulence. In terms of the invariants, the axisymmetric turbulence can be represented by

$$III = \pm 2(-II/3)^{3/2}, \tag{17}$$

where the positive sign is for cigar-shaped turbulence, and the negative sign is for pancake-shaped turbulence.

The classification of turbulence used in the present study is based on the shape of the energy ellipsoid (Lumley & Newman 1977; Lumley 1978). The energy ellipsoid of homogeneous turbulence after an axisymmetric contraction has a pancake shape, since one component of the turbulent kinetic energy is smaller than the other two. In an axisymmetric contraction the turbulence eddies are stretched in the axial direction, making them a rod-like shape (Lee & Reynolds 1985). On the other hand, the energy ellipsoid of turbulence after an axisymmetric expansion has a cigar shape since one component of turbulent kinetic energy is greater than the other two. In this case, however, the turbulence eddies seem to have neither unique structure nor preferred direction as the turbulence is compressed in the axial direction while stretched in the other directions (Rogers & Moin 1987). It must be pointed out here that Reynolds & Kassinos (1995) classify turbulence based on the shape of turbulence eddies rather than the shape of energy ellipsoid as used here. In their system of classification, therefore, the 2-D isotropic state of turbulence at the left-hand corner of the turbulence triangle (see figure 1) is called two-component/two-dimensional turbulence, while the 1-D state of turbulence at the right-hand corner is called one-component/two-dimensional turbulence.

The first part of the present experiment was designed in such a way that the homogeneous anisotropic turbulence would follow the ordinate of figure 1 toward the origin, corresponding to the 3-D isotropic turbulence. The second part of the experiment was planned to correspond to where the turbulence would return to isotropy along the right-hand side of the triangle toward the origin. In the last part of the experiment, pancake-shaped turbulence for different Reynolds numbers was generated, and the behaviour of homogeneous turbulence in returning to isotropy along the left-hand side of the turbulence triangle was investigated.

3. Experimental set-up and procedure

3.1. *Experimental set-up*

An open-return wind tunnel (Choi 1983) was used for the first two parts of the present study, the plane distortion and the axisymmetric expansion experiments. First, air was passed down to a blower through air filters. A flat layer of glass wool was placed at

the intake of the blower, followed by a layer of bag filters. Dust, mist and oil particles greater than 1 μm in diameter were removed from the intake air after passing through these filters. The filtered air then went through a bell-mouth into a centrifugal blower, whose outlet (0.21 m × 0.25 m in cross-section) was connected to a series of acoustic mufflers through thick layers of rubber to prevent direct transmission of mechanical vibration. The first muffler was of expansion-chamber type (Kinsler & Frey 1962) with its chamber lined with 0.10 m thick acoustic foam. The second was a Helmholtz resonator mounted as a side branch on top of a square duct. A 0.15 m long honeycomb with a 9.5 mm hexagonal cell was fitted in the duct following the Helmholtz resonator in order to straighten the incoming flow from the blower and to reduce the turbulence level. The honeycomb section was followed by a preliminary diffuser, and then by a main diffuser. There were two screens of 0.19 mm diameter wires with solidity $\sigma = 0.35$ in the 0.30 m long preliminary diffuser, whose cross-sectional area was increased form 0.21 m × 0.25 m to 0.30 m × 0.30 m. In the 0.61 m long main diffuser section, seven screens were placed to prevent the flow separation. They were placed in such a way that the pressure rise between the neighbouring screens could be cancelled by the pressure drop at a screen that follows. The main diffuser was followed by a 0.58 m long settling chamber of 1.22 m × 1.22 m cross-section, where eight fine-mesh screens of 0.17 mm diameter wires ($\sigma = 0.43$) were equally spaced. A 0.89 m long smooth contraction of the flow then took place following the settling chamber. The width of the contraction section was reduced from 1.22 m to 1.02 m, while the height was reduced from 1.22 m to 0.127 m, both two-dimensionally, resulting in a contraction ratio of 11.5. After the contraction section, the flow passed through a turbulence-generating grid made of 3.18 mm thick square brass tubes in a bi-plane structure. The mesh length of the turbulence grid was 14.0 mm with solidity of 0.403. Following a 0.28 m long straight-duct section after the grid, the turbulence was subjected to an irrotational distortion in the distorting duct (Tucker 1970). The grid-generated turbulence travelled for 45 mesh lengths in the distorting duct in order to relax from the initial inhomogeneity and anisotropy while it was strained. At the end of the distorting duct, the turbulence was suddenly relaxed from the irrotational strain in a 2.45 m long test section. The cross-sectional dimension of the test section was 0.254 m × 0.508 m for the plane distortion experiment, and 0.254 m × 0.254 m for the axisymmetric expansion experiment. The top wall of each test section was made of flexible Plexiglas, allowing the height along the section to be continuously adjusted to maintain a constant mean velocity. The mean velocity was set at 21.0 m s^{-1} for the plane distortion experiment, and 11.5 m s^{-1} for the axisymmetric expansion experiment. There were 22 test holes along the test section, 19 of which were at the side and three at the bottom, through which hot-wire probes were inserted. All the measurements were carried out along the centerline of the test section. A layer of screen was placed at the end of the test section in order to avoid premature divergence of the flow from the test section. The background turbulence level of the wind tunnel in the test section was about 0.2%.

The wind tunnel used for the axisymmetric contraction experiment was of vertically oriented, open-return type with a 9 : 1, three-dimensional contraction (Warhaft 1980). A turbulence-generating grid with solidity of 0.34 was placed after the main contraction section, which was followed by the second contraction section. This double-contraction configuration allowed us to generate pancake-shaped axisymmetric turbulence with different initial Reynolds number and anisotropy. The second contraction section leading to the 2.57 m long test section was a scaled-down version of the main contraction, where the 0.20 m long section was reduced from

0.406 m × 0.406 m to 0.203 m × 0.203 m. The turbulence level in the vertical wind tunnel was less than 0.2%. Further details of the wind tunnels together with the flow parameters and turbulence characteristics are given in table 1.

3.2. *Experimental procedure*

The data acquisition system employed in the present experiment is the same as that used by Warhaft (1980) and Sirivat (1983). Two channels of amplified AC signals from an X-wire sensor were converted to digital signals by a 12-bit A/D converter at $\pm$5 V full scale, and sent to the PDP 11/34 mini-computer. The computer sampled a block of data, consisting of 1024 data points, into the buffer memory at a time and paused between blocks to write them onto the hard disk. After one hundred blocks of data equivalent to 102 400 data points were sampled, they were copied to a magnetic tape. The tape was later replayed and analysed using the STAT program developed by Kaminski and Warhaft (Kaminski 1978).

The first two parts of the present study, the plane distortion experiment and the axisymmetric expansion experiment, were carried out using hot wires with a DISA 56C01/16 constant-temperature anemometer (CTA) system and DISA 56N20 signal conditioners. Hewlett Packard 3466A digital multimeters were also used for reading the mean output voltages from the CTA system. AC signals from the CTA were amplified and filtered by signal conditioners at 10 Hz for high pass, and at 10 kHz for low pass before being sent to the computer for sampling. The low-pass filter was set at the Nyquist frequency to avoid the aliasing of the sampled data. The turbulent kinetic energy lost during the low-pass filtering process is estimated to be less than 0.2% of the total energy. We do not expect much energy in the turbulence below 10 Hz since the length scale of the largest turbulence eddies should be no more than the width of the test section (0.254 m), which roughly corresponds to the high-pass filtering frequency. In some cases, two sets of data acquisition were performed with different band-filter settings, and the two energy spectra were patched together, covering a wide frequency range between 0.75 Hz and 7 kHz. The background noise of the wind tunnel was compensated for by subtracting the energy spectrum of an empty wind tunnel from the measured energy spectra.

We have modified the DISA 55P51 X-wires for velocity measurements by soldering a 3.0 mm long, copper-plated tungsten wire between the prong tips, which was then etched at its centre to make a 0.45 mm long sensitive section with 3 μm diameter. The separation between the neighbouring wires was 0.90 mm. The over-heat ratio of the hot wires was set to a constant value of 1.8 throughout the measurements. In the axisymmetric contraction experiment, a DISA 55M01/05/10 CTA system and Krohnhite 3342 filters were used instead. Hot-wire calibration was performed in a small calibration tunnel that was designed and built especially for this purpose. The tunnel was warmed up long before calibrations were done so that the air temperature was constant throughout the measurements. Whenever the hot-wire characteristics were found to have significantly changed after a run of experiments, all the acquired data were discarded. Otherwise, an averaged value of the two sets of the calibration, one obtained before the experiment and the other after, was used for the reduction of experimental data. A standard static calibration method for hot wires was employed (Bradshaw 1975; Perry 1982), where the functional relationship between the flow velocity and the output DC voltage from the CTA system was fitted to King's law. The effective cooling velocity was determined using an expression given by Champagne, Sleicher & Wehrmann (1967), where the yaw factor was obtained for each wire as a function of the yaw angle at the same Reynolds number as the

Quantity		Plane distortion ($x/M = 73.8$)	Axisymmetric expansion ($x/M = 73.8$)	Axisymmetric contraction		
				Set 1 ($x/M = 87.4$)	Set 2 ($x/M = 39.4$)	Set 3 ($x/M = 39.4$)
$\overline{q^2}/\bar{U}^2 = A(x/M + B)^{-n}$	A	1.33×10^{-1}	1.92×10^{-2}	5.26×10^{-4}	5.72×10^{-2}	4.70×10^{-4}
	B	39.9	66.6	70.2	74.6	45.6
	n	1.06	0.756	0.634	1.22	0.401
$\bar{U}(\mathrm{m\,s^{-1}})$		21.0	11.5	17.5	17.7	20.2
$M(\mathrm{m})$		0.0140	0.0140	0.00847	0.0250	0.0250
R_l		206	342	10.6	105	116
ρ^*		1.20	0.882	0.634	2.14	1.12
II		-0.76×10^{-2}	-1.97×10^{-2}	-2.67×10^{-2}	-1.79×10^{-2}	-4.28×10^{-2}
III		0.17×10^{-3}	1.00×10^{-3}	-1.69×10^{-3}	-0.92×10^{-3}	-3.39×10^{-3}

TABLE 1. Characteristic turbulence parameters in the present experiment.

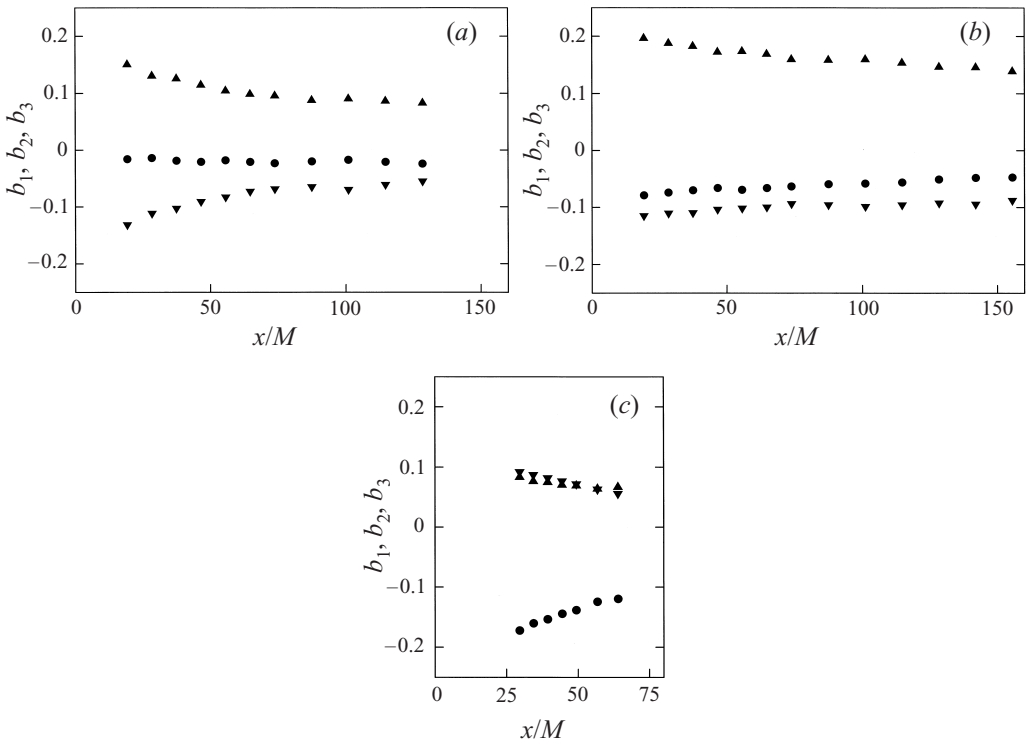

FIGURE 2. Development of the principal values of the anisotropy tensor after (*a*) plane distortion, (*b*) axisymmetric expansion, and (*c*) axisymmetric contraction: ●, b_1; ▲, b_2; ▼, b_3.

individual experiment. The effect of the pitch angle on the effective cooling velocity was very small (Jorgensen 1971), usually negligible.

In the present experiment, the Kolmogorov microscale κ of turbulence was of the order of the sensitive wire length δ of the hot-wire probe. This might have caused an error by underestimating the turbulent kinetic energy near the Kolmogorov frequency $f_\kappa = \bar{U}/2\pi\kappa$. Wyngaard (1968) showed for a hot wire whose wire separation is equal to the sensitive wire length that the longitudinal and the lateral one-dimensional energy spectra are underestimated by 5% and 10%, respectively, at the frequency $f_l = \bar{U}/2\pi l$. Although these errors seem to be large, the contribution to the total turbulent kinetic energy is very small since the energy spectra tail off sharply at higher frequencies. In fact, only 1% of the total turbulent kinetic energy is contained above the frequency $f_\delta = \bar{U}/2\pi\delta$ in the present experiment.

4. Results and discussion

4.1. *Development of characteristic properties*

The development of the principal values of the anisotropy tensor is given in figures 2(*a*), 2(*b*) and 2(*c*) for the plane distortion, axisymmetric expansion and axisymmetric contraction experiments, respectively. The trace of the anisotropy tensor is zero so that these values represent the degree of anisotropy in each principal direction. The figures demonstrate that the rate of return to isotropy is quite different among the experiments. The anisotropic turbulence after the axisymmetric contraction (figure 2*c*) seems to have the fastest rate of return to isotropy, while the turbulence after the

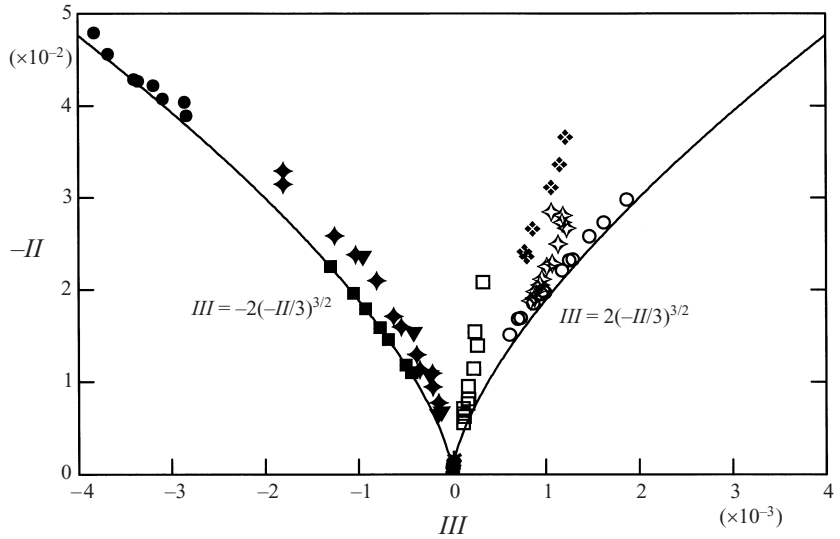

FIGURE 3. The trajectories of the return to isotropy of homogeneous turbulence in invariant coordinates: □, present experiment (plane distortion); ○, present experiment (axisymmetric expansion); ■, present experiment (axisymmetric contraction, set 2); ●, present experiment (axisymmetric contraction, set 3); ❖, Gence & Mathieu (1980); ✧, Le Penven *et al.* (1985) $III > 0$; ✦, Le Penven *et al.* (1985) $III < 0$; ▼, Tucker (1979); ⁎, Comte-Bellot & Corrsin (1966).

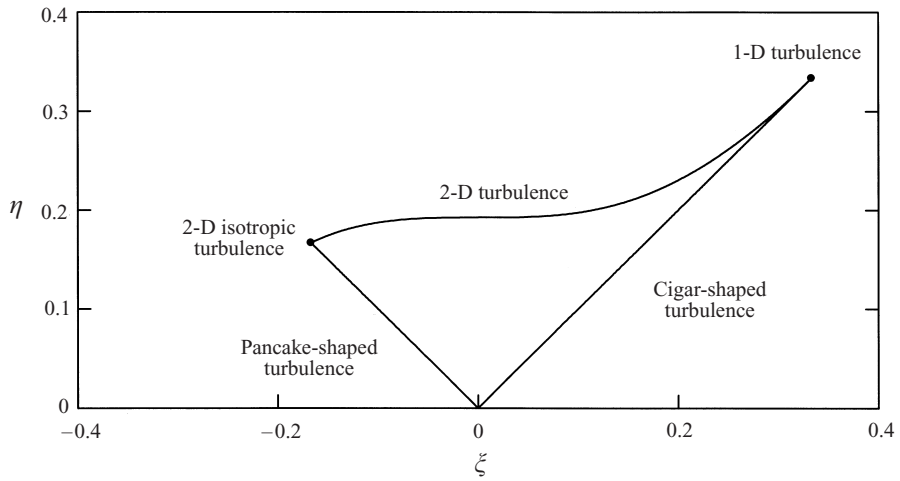

FIGURE 4. The turbulence triangle and possible states of turbulence in invariant coordinates, η vs. ξ.

plane distortion (figure 2*a*) has a faster rate of return than that after the axisymmetric expansion (figure 2*b*). It is also shown that the rate of return to isotropy is different for different principal directions in each case. For example, the intermediate principal value in the plane distortion experimental (figure 2*a*) barely returns to isotropy, while the other two principal values show significant rates of return. This provides experimental evidence that the return to isotropy is not a linear process. Figure 3 shows a plot of these results along with the other experimental results in the invariant coordinates ($-II$ vs. III), demonstrating that the anisotropic turbulence created in the present experiment was very similar to what we had initially expected.

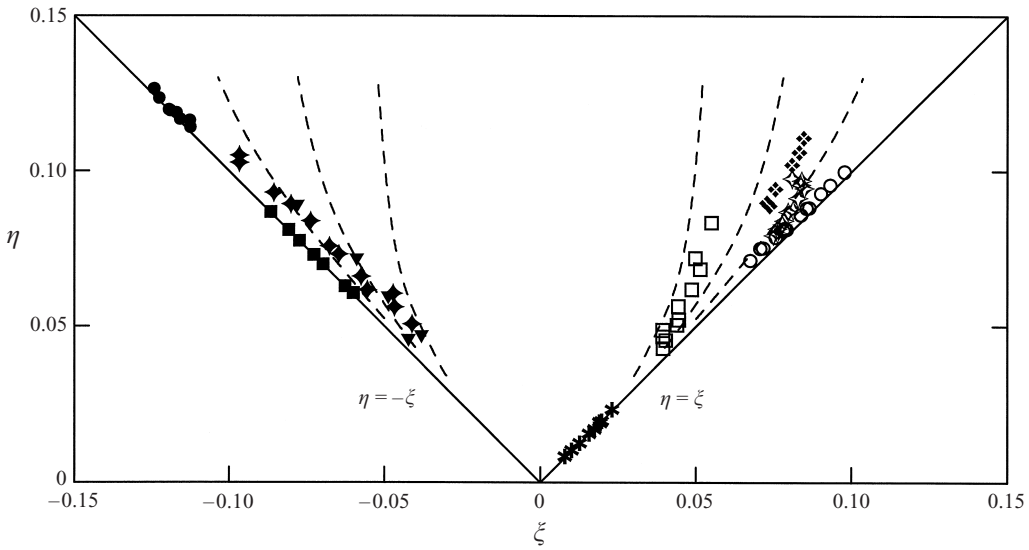

FIGURE 5. The trajectories of the return to isotropy of decaying homogeneous turbulence in the ξ–η coordinates. Symbols are as in figure 3. Dashed lines are the predictions by the present turbulence model of § 4.3.

In order to see the nonlinear behaviour in the return to isotropy more clearly and to examine the trajectories of the return to isotropy of homogeneous turbulence, we introduce new variables ξ and η (Choi 1983) defined by

$$\xi^3 = III/2, \quad \eta^2 = -II/3. \tag{18}$$

The turbulence triangle can also be transformed from the III–$(-II)$ coordinates (figure 1) to the ξ–η coordinates in figure 4. As will be discussed later in § 4.3, any nonlinearity in the return to isotropy of homogeneous turbulence can be seen from the turbulence trajectories in the ξ–η coordinates. In other words, the trajectories of anisotropic turbulence should be straight lines through the origin if Rotta's model for a linear return to isotropy were correct (Choi 1983). All the available experimental data, in which all three components of turbulent kinetic energy were measured, are plotted in figure 5. It can be seen in this figure that the turbulence trajectories are not straight lines through the origin, indicating that the return to isotropy of anisotropic turbulence is indeed a nonlinear process. Evidently, turbulence wants to become axisymmetric ($\eta = \pm\xi$ corresponds to axisymmetry) even more than it wants to become isotropic. This nonlinearity is most clearly seen from the data with $III > 0$ in the present experiment after the plane distortion, in Gence & Mathieu (1980) and in Le Penven *et al.* (1985). It is, however, less clear from the data with $III < 0$ in Tucker (1970) and Le Penven *et al.* (1985).

The decay process of turbulent kinetic energy can be expressed quite well by a power law. The powers and other constants in the decay law of turbulent kinetic energy are given in table 1. The table also shows the characteristic flow parameters in the present experiment. It is shown that the Reynolds numbers based on the turbulence length scale and the velocity scale of energy-containing eddies, as defined in equation (9), are of the same order for all the experiments except for set 1 of the axisymmetric contraction experiment, whose Reynolds number was much smaller than the rest. In this set of experiment, a fine mesh grid with $M = 8.47$ mm was placed

60 mesh lengths upstream of the second contraction section, so that the turbulence velocity scale as well as the turbulence length scale were small compared with those in other sets of the present experiment. This difference in the Reynolds number helped determine the functional dependence of the Reynolds number on the rate of return to isotropy of homogeneous anisotropic turbulence. We were also able to compare these experimental results with the direct numerical simulation data, which were obtained at Reynolds numbers that were more than an order of magnitude lower. The details of these procedures, together with the discussion of the effect of the Reynolds number on the rate of return, are given later in § 4.5.

Table 1 also shows that the degree of anisotropy of turbulence, measured either by II or III, was quite different between sets 2 and 3 of the axisymmetric contraction experiment. The degree of anisotropy in set 2 was smaller and is similar to that of Mills & Corrsin (1957) and Uberoi (1957), while the turbulence in set 3 had a greater anisotropy, similar to that of Uberoi (1956) and Warhaft (1980). This difference in the degree of anisotropy came from the fact that the grids were placed at different upstream positions from the second contraction section. In set 3 a coarse grid with $M = 25.0$ mm was placed 60 mesh lengths upstream of the beginning of second contraction section. Hence the grid-generated turbulence had enough time to relax before it was strained in the second axisymmetric contraction section. In set 2, however, the same coarse grid was placed 20 mesh lengths upstream of the second contraction section. In other words, the initial cigar-shaped turbulence from the grid reached the second axisymmetric contraction before it became nearly isotropic, which takes approximately 50 mesh lengths (Warhaft 1980). As a consequence, the degree of anisotropy of set 2 of the axisymmetric contraction experiment was much smaller than that of set 3.

4.2. *The rate of the return to isotropy*

In figure 6 the characteristic time scale ratio ρ^* is plotted for all the available data against the function F defined in (16). The parameter ρ^* is defined as the ratio of the two time scales of turbulence – the time scale for the decay of the turbulent kinetic energy $\overline{q^2}/\mathrm{d}\overline{q^2}/\mathrm{d}t$ and the time scale for the return to isotropy $II/\mathrm{d}II/\mathrm{d}t$:

$$\rho^* = \frac{\overline{q^2}/\mathrm{d}\overline{q^2}/\mathrm{d}t}{II/\mathrm{d}II/\mathrm{d}t}. \tag{19}$$

The characteristic time scale ratio ρ^* can be interpreted as a measure of the rate of return to isotropy of anisotropic turbulence in a normalized time space, which takes a greater value when the return to isotropy is faster. The Reynolds numbers for all the data shown in figure 6 are of the same order except for set 1 of the present axisymmetric contraction experiment and for the DNS data of Rogallo (1981), whose Reynolds numbers are more than an order of magnitude smaller than the rest. Figure 6 demonstrates that the rate of return to isotropy of anisotropic turbulence after the axisymmetric expansion (whose trajectory is on the right-hand side of the turbulence triangle in figures 1 and 4) is the slowest, and it becomes faster as the corresponding turbulence trajectory moves toward the left-hand side of the turbulence triangle. The rate of return to isotropy of turbulence after the plane distortion is faster than that of the axisymmetric expansion, and it is fastest after the axisymmetric contraction, confirming the finding of Gence & Mathieu (1980). The rate of the return to isotropy for set 1 of the present axisymmetric contraction experiment was as low as Rogallo's data.

In order to help visualize the difference in the rate of return to isotropy as a

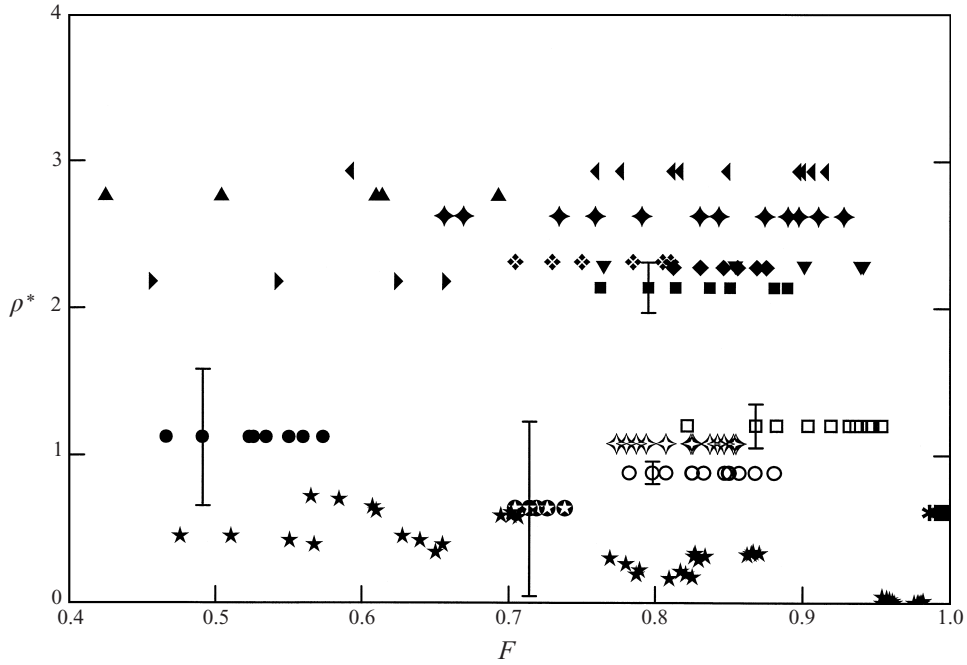

FIGURE 6. The characteristic time-scale ratio ρ^* as a function of F: ✪, present experiment (axisymmetric contraction, set 1); ▲, Warhaft (1980); ◆, Mills & Corrsin (1959); ►, Uberoi (1956); ◄, Uberoi (1957); ★, Rogallo (1981). The other symbols are as in figure 3. Experimental error is indicated by error bars in terms of the 90% confidence level.

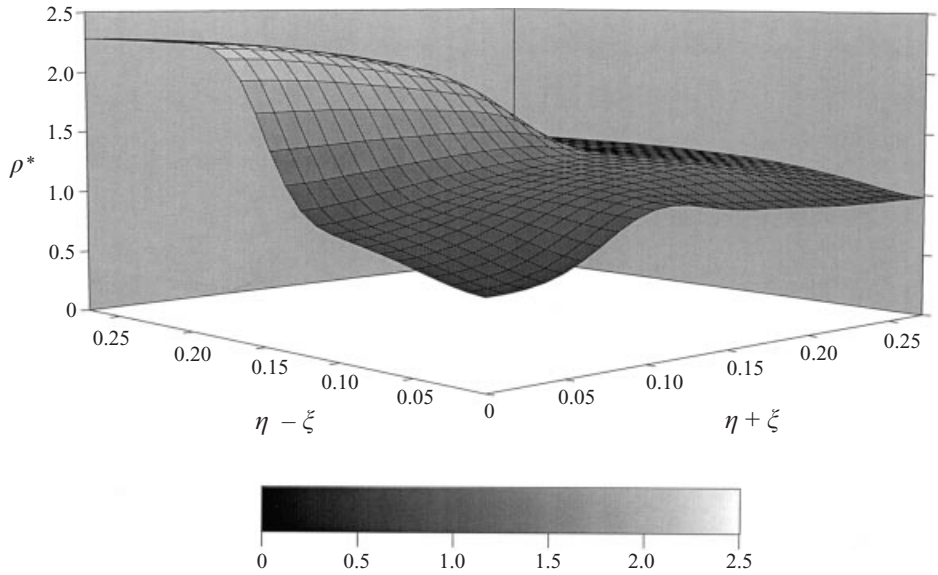

FIGURE 7. Surface map for the characteristic time-scale ratio ρ^* plotted against $(\eta + \xi)$ and $(\eta - \xi)$ coordinates. The straight lines given by $\eta = \xi$ and $\eta = -\xi$ correspond to right- and left-hand sides of the turbulence triangle in figures 4 and 5, representing cigar-shaped and pancake-shaped turbulence, respectively.

Experiment	n	B	$\sqrt{R_l}$	$2\bar{U}\tau_\kappa/M$	Location of data (x/M)
Plane distortion	1.06	39.9	14	3.58	20–128
Axisymmetric expansion	0.756	66.6	18	6.53	20–156
Axisymmetric contraction					
Set 1	0.634	70.2	3.3	44.7	59–117
Set 2	1.22	74.6	10	8.15	30–64
Set 3	0.401	45.6	11	13.8	20–57

TABLE 2. Non-dimensional distance for dissipation to return to isotropy.

function of the type and degree of anisotropy of turbulence, a surface map for ρ^* is plotted against $(\eta + \xi)$ and $(\eta - \xi)$ in figure 7 using all the available data. The straight lines given by $\eta = \xi$ and $\eta = -\xi$ in this figure correspond to the right- and left-hand sides of the turbulence triangle (figures 4 and 5), representing cigar-shaped and pancake-shaped turbulence, respectively.

Random experimental error in terms of the 90% confidence level is indicated by error bars in figure 6, where we note that some of the experimental data have large scatter. It was initially suspected that the scatter in the characteristic time-scale ratio ρ^* among the experimental data was partly due to the anisotropy of dissipation. In order to evaluate the effect of anisotropy of dissipation on the rate of return to isotropy of turbulent kinetic energy, we estimated the non-dimensional distance required for dissipation to return to isotropy by

$$2\bar{U}\tau_k/M = \frac{4}{3n}\left(\frac{x}{M} + B\right)\frac{1}{\sqrt{R_l}}. \tag{20}$$

Here, we assumed that the time scale for dissipation to return to isotropy is about twice the dissipation time scale, which is given by

$$\tau_k = (\nu/\bar{\varepsilon})^{1/2} = \frac{1}{3}\frac{\overline{q^2}}{\bar{\varepsilon}}\frac{1}{\sqrt{R_l}}, \tag{21}$$

where the rate equation for turbulent kinetic energy is given (Tennekes & Lumley 1972) by

$$\mathrm{d}\overline{q^2}/\mathrm{d}t = -2\bar{\varepsilon}, \tag{22}$$

and the power-decay law of turbulent kinetic energy by

$$\frac{\overline{q^2}}{\bar{U}^2} = A\left(\frac{x}{M} + B\right)^{-n}. \tag{23}$$

The values for $2\bar{U}\tau_k/M$ in equation (20) are calculated for each experiment at the end of the distortion section and are shown in table 2. Also shown in the table is the location in the test section where the measurements were taken in each experiment. It is clear from the table that all the measurements in the present experiment were taken after the dissipation had returned to isotropy. In other words, the time scale for dissipation to return to isotropy is much smaller than that for turbulent kinetic energy. This is in good agreement with a recent result of direct numerical simulation by Ikai & Kawamura (1995). Therefore, the effect of initial anisotropy of dissipation on the rate of return to isotropy of turbulent kinetic energy is negligible in the present set of experimental data.

Kassinos & Reynolds (1997) pointed out that the anisotropy of cigar-shaped turbulence developed under a relatively slow expansion such as in the present study is greater than the limiting value predicted by the rapid distortion theory. This was also observed by Lee (1986) in his DNS study of homogeneous turbulence as well as in an experiment on an impinging jet near the stagnation region (Nishino *et al.* 1996). The rapid distortion theory, of course, neglects viscosity and nonlinear scrambling (Batchelor & Proudman 1954), so it might be expected to predict greater, not less, anisotropy after the expansion. This curious finding deserves explanation.

Our expectation of rapid distortion theory is apparently simplistic, since the result of both experiment and numerical simulation, even at the very low Reynolds number of the computation, indicate greater anisotropy than predicted by the distortion theory. This suggests, first, that the rapid distortion theory is a poor yardstick with which to gauge turbulence. It also suggests that the nonlinear scrambling neglected in the rapid distortion theory is much more complicated than a simple relaxation. It seems unlikely, however, that the neglect of viscous dissipation is the culprit.

The present experiment shows that the return to isotropy is very slow for cigar-shaped turbulence under the axisymmetric expansion. On the other hand, the DNS study conducted by Lee (1986) demonstrated the surprising result that upon removal of the strain the anisotropy of the Reynolds stress continued to increase. This overshoot in the anisotropy was found, however, only in a case where the strain rate was very large, by more than an order of magnitude, compared to the experiment. All the other cases studied by Lee (1986) and the DNS results by Yamamoto (1985) indicate that cigar-shaped turbulence returned towards isotropy monotonically without an overshoot.

It is certainly difficult to imagine that this discrepancy can be explained by the lack of precise homogeneity or axisymmetry in the present experiment. The measured turbulence homogeneity of the present study is as good as other experiments of this type (Le Penven *et al.* 1985). Indeed, the variation in the mean velocity in the test section after the axisymmetric expansion duct was less than $\pm 1\%$ within ± 4 mesh lengths, while the turbulence intensity was uniform within $\pm 4\%$. The axisymmetry of cigar-shaped turbulence was also good as indicated by the value of $\xi/\eta = 0.95$, where $\xi = \pm\eta$ corresponds to the axisymmetric state of turbulence. The DNS data are probably also not precisely axisymmetric or homogeneous, since it is a single realization.

We believe that the remarkably low Reynolds number of the DNS study combined with the large strain rate applied to the turbulence may be the explanation for the difference. The behaviour of the experimental data is consistent with that of the DNS, in the sense that cigar-shaped, axisymmetric turbulence at a higher Reynolds number shows a very slow return towards isotropy, while the DNS result under a rapid expansion shows a negative return. This is the sort of difference that could be induced by a considerable difference in the Reynolds number and the strain rate. One would have to image the rate of return of cigar-shaped turbulence increasing as the Reynolds number increased and the strain rate decreased, beginning from negative values. Evidently, at least under some circumstances, 'return to isotropy' is a misnomer. To model this complex behaviour, a thoroughly nonlinear dependence on the anisotropy tensor b_{ij} would work, including the third invariant. Lacking that, possibly a dependence on the time derivative of the anisotropy tensor might work.

In a recent report, Kassinos & Reynolds (1997) have suggested another explanation for the discrepancy by introducing a new type of turbulence model. Their model parameterizes the turbulence not only by the anisotropy tensor but also by two other

similar tensor that describe the physical structure, rather than the velocity structure – essentially the anisotropy of streamline spacing. Each of these tensors has its own relaxation rate, and the differential relaxation results in the fast growth of anisotropy, leading to an overshoot under a rapid expansion, which has been observed in the DNS study (Lee 1986). This is a plausible explanation for the discrepancy discussed above, and indeed their model correctly predicts this behaviour. However, this is a complex, highly speculative and relatively untested model. It needs to be verified with many more flows, and be evaluated by the research community, before it can be fully trusted. However, this model is certainly an interesting one, and does directly address the sort of mechanism that must be at play in the return to isotropy of homogeneous turbulence.

4.3. *Trajectories of the return to isotropy*

Using the results of the present experiments along with others (Tucker 1970; Gence & Mathieu 1980; Le Penven *et al.* 1985), we are able to show that the return to isotropy of homogeneous turbulence does not follow Rotta's linear model (Rotta 1951). In other words, the turbulence trajectories in figure 5 are not straight lines through the origin, indicating that the return to isotropy is a nonlinear process. This can be shown as follows.

The behaviour of turbulence trajectories shown in figure 5 can be expressed by

$$0 \leqslant \frac{|\xi|}{\eta} \leqslant 1, \tag{24}$$

$$0 \leqslant \frac{\mathrm{d}\ln|\xi|}{\mathrm{d}\ln\eta} \leqslant 1. \tag{25}$$

and

$$\frac{\mathrm{d}\ln|\xi|}{\mathrm{d}\ln\eta} \to 0 \quad \text{as} \quad \frac{|\xi|}{\eta} \to 0 \tag{26}$$

where, ξ and η are defined in (18) as

$$\xi^3 = III/2, \quad \eta^2 = -II/3.$$

We now use the rate equations for the second and the third invariants, which are respectively given by

$$\frac{\mathrm{d}II}{\mathrm{d}\tau} = -2(\beta - 2)II + 3\gamma III, \tag{27}$$

$$\frac{\mathrm{d}III}{\mathrm{d}\tau} = -3(\beta - 2)III - \tfrac{2}{3}\gamma II^2. \tag{28}$$

These equations are obtained by substituting (14) into (8), after using the definitions for the invariants, (12). Equations (27) and (28) are combined to give

$$\frac{\mathrm{d}\ln|\xi|}{\mathrm{d}\ln\eta} = \frac{\mathrm{d}\ln|III^{1/3}|}{\mathrm{d}\ln(-II)^{1/2}} = \frac{2II\,\mathrm{d}III/\mathrm{d}\tau}{3III\,\mathrm{d}II/\mathrm{d}\tau} = \frac{1 + GX^{-4}}{1 + GX^2}. \tag{29}$$

Here, functions G and X are defined by

$$G = \frac{\gamma}{(\beta - 2)}\xi \tag{30}$$

and

$$X = \frac{\xi}{\eta}. \tag{31}$$

The function G is essentially a measure of the relative magnitude of the nonlinear and linear return to isotropy of homogeneous turbulence. In other words, $G = 0$ in Rotta's model. In this case, equation (29) reduces to

$$\frac{\mathrm{d}\ln|\xi|}{\mathrm{d}\ln\eta} = 1.$$

This is an equation for a family of straight lines through the origin. In other words, the turbulence should follow straight lines through the origin if Rotta's model for the linear return to isotropy were correct (Choi 1983).

Substituting (29) into (25) and (26) and using (24), we find the following functional behaviour for G:

$$-X^4 \leqslant G \leqslant 0 \tag{32}$$

and

$$G \to -X^4 \quad \text{as} \quad X \to 0. \tag{33}$$

The following simple function for G satisfies both equations (32) and (33):

$$G = -X^4 + hX^6, \quad 0 \leqslant h \leqslant 1, \tag{34}$$

where $h = 0.8$ gives the best fit to the experimental data. The trajectories of the return to isotropy predicted by this model are shown with dashed lines in figure 5.

The return to isotropy tensor in (14) can be written as

$$\phi_{ij} = (\beta - 2)\left[b_{ij} + \frac{\gamma}{(\beta-2)}(b_{ik}\,b_{kj} + \tfrac{2}{3}II\,\delta_{ij})\right] + 2b_{ij}, \tag{35}$$

where the ratio of the two unknown invariant functions γ and $(\beta - 2)$ is modelled using (30) and (34) as

$$\frac{\gamma}{(\beta-2)} = \frac{G}{\xi} = \frac{-X^4 + 0.8X^6}{\xi}. \tag{36}$$

Equation (35) for the return-to-isotropy tensor ϕ_{ij} now contains only one unknown invariant function β. We can write the characteristic time scale ratio ρ^* in terms of the non-dimensional time τ defined in (6) as

$$\rho^* = -\frac{1}{2}\frac{\mathrm{d}II}{\mathrm{d}\tau}/II. \tag{37}$$

Substituting (27) into (37) we obtain

$$\rho^* = (\beta - 2)\left[1 - \frac{3}{2}\frac{G}{\xi}\frac{III}{II}\right] = (\beta - 2)(1 + GX^2). \tag{38}$$

Equation (38) relates the only unknown invariant function β to an experimentally obtainable quantity ρ^*, which is shown in figure 6 for all the available experimental data. Substituting (38) into (35), we obtain

$$\phi_{ij} = \frac{\rho^*}{(1 + GX^2)}\left[b_{ij} + \frac{G}{\xi}(b_{ik}\,b_{kj} + \tfrac{2}{3}II\,\delta_{ij})\right] + 2b_{ij}, \tag{39}$$

where G is given by (34) as

$$G = -X^4 + 0.8X^6.$$

By substituting (39) into (8), the rate equation for the anisotropy tensor b_{ij} can be

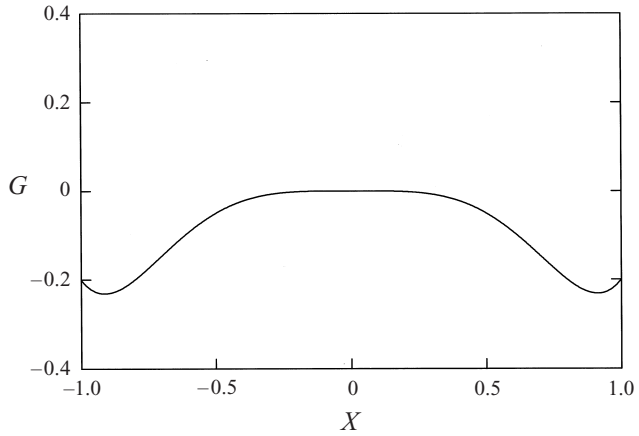

FIGURE 8. Function G vs. X to show a nonlinear return to isotropy of homogeneous turbulence.

expressed by

$$\frac{\mathrm{d}b_{ij}}{\mathrm{d}\tau} = -\frac{\rho^*}{(1+GX^2)}\left[b_{ij} + \frac{G}{\xi}(b_{ik}\,b_{kj} + \tfrac{2}{3}II\,\delta_{ij})\right]. \tag{40}$$

It has already been mentioned that the function G is a measure of the relative magnitude of the nonlinear and linear return to isotropy of homogeneous turbulence. This can be easily demonstrated by expanding (39) in G as

$$\phi_{ij} = (\rho^* + 2)b_{ij} - \rho^* G\left[X^2 b_{ij} - \frac{b_{ik}\,b_{ki} + \frac{2}{3}II\,\delta_{ij}}{\xi}\right] + O(G^2). \tag{41}$$

The function G is plotted versus X in figure 8, indicating that the nonlinear effect is significant for $|X| \geqslant 0.5$.

The symmetry condition for the trajectories of the return to isotropy of homogeneous turbulence can be stated thus: the turbulence must stay axisymmetric once it becomes axisymmetric. In other words, the turbulence cannot distinguish the two principal values of the Reynolds stress tensor once they become identical. Stating this in the invariant coordinates, the decaying turbulence must return to isotropy along the right- or left-hand side of the turbulence triangle toward the origin once it touches either of these sides. This can easily be shown by taking a time derivative of the following function:

$$f(II, III) = \left(-\frac{II}{3}\right)^{1/2} - \left|\frac{III}{2}\right|^{1/3}. \tag{42}$$

This function $f(II, III)$ becomes zero if and only if turbulence is axisymmetric. Using (27) and (28), we can easily obtain that

$$\frac{\mathrm{d}}{\mathrm{d}\tau} f(II, III) = 0 \quad \text{as} \quad f(II, III) \to 0. \tag{43}$$

Our experimental results demonstrated (figures 3 and 5) that the axisymmetric turbulence, whether it is cigar-shaped or pancake-shaped, stayed axisymmetric as it returned toward isotropy. In other words, it returned towards the origin (three-dimensional isotropic state of turbulence) along the right- or left-hand side of the turbulent trian-

gle. Makita & Minami (1995) also confirmed the above symmetry condition for the trajectories of cigar-shaped axisymmetric turbulence.

We now examine the behaviour of trajectories for the return to isotropy of homogeneous turbulence which is initially on $III = 0$ ($\xi = 0$). From (28), we have

$$\frac{\mathrm{d}III}{\mathrm{d}\tau} = -\tfrac{2}{3}\gamma II^2 \tag{44}$$

for the turbulence whose third invariant III is initially zero ($\xi = 0$). The term on the right-hand side of this equation does not vanish unless the second invariant II becomes zero (three-dimensional isotropic turbulence) or γ vanishes. We do not know *a priori* whether γ vanishes or not as the third invariant becomes zero. Hence the turbulence, which is initially on $III = 0$ ($\xi = 0$), does not necessarily return to isotropy along $III = 0$ ($\xi = 0$). The present turbulence model is an even function in ξ, hence it is an even function in III. Therefore, this model predicts the decaying homogeneous turbulence to return to isotropy along $III = 0$ once III becomes zero. This is in contrast to the quadratic model for the return to isotropy of homogeneous turbulence (Sarkar & Speziale 1990), where the invariant functions γ and (β-2) are set to constant values. This makes G in (30) an odd function in ξ. Therefore, the trajectories of decaying turbulence predicted by the quadratic model are not symmetric with respect to the ordinate ($III = 0$).

4.4. *Realizability conditions for turbulence models*

The concept of realizability in second-order modelling is introduced by Schumann (1977). He proposed three realizability conditions for the Reynolds stress tensor $R_{ij} = \overline{u_i u_j}$:

$$R_{\alpha\beta} \geqslant 0 \quad \text{for} \quad \alpha = \beta, \tag{45}$$

$$R_{\alpha\beta}^2 \leqslant R_{\alpha\alpha} R_{\beta\beta} \quad \text{for} \quad \alpha \neq \beta, \tag{46}$$

$$\det(R_{\alpha\alpha}) \geqslant 0. \tag{47}$$

Equation (45) requires non-negative, component turbulent kinetic energies, while (46) is the consequence of Schwartz' inequality. Equation (47) requires that the Reynolds stress tensor must be real. The turbulence model must satisfy these conditions in order to guarantee a realizable solution from numerical simulations. This concept is especially important in computations when the initial conditions are so poor that there are chances for component energies to become negative. It is also important when we deal with turbulent flows in which one of the component turbulent kinetic energies is suppressed to become nearly two-dimensional (Lumley 1978). The best way to implement these conditions in our model is to work with the function F defined in (16). It is easy to show that F is 27 times the product of the three eigenvalues of the Reynolds stress tensor normalized by the turbulent kinetic energy; therefore it vanishes if and only if one of the component energies vanishes. In order to guarantee that none of the eigenvalues of the Reynolds stress tensor become negative, we require that

$$\frac{\mathrm{d}F}{\mathrm{d}\tau} \to 0 \quad \text{as} \quad F \to 0. \tag{48}$$

Using (27) and (28), the time derivative of F can be given by

$$\frac{\mathrm{d}F}{\mathrm{d}\tau} = -9\frac{\rho^*}{(1+GX^2)}\left[\left(9III + 2\frac{G}{\xi}II^2\right) + 2(1+GX^2)II\right]. \tag{49}$$

Therefore, if we choose ρ^* such that

$$\rho^* \to 0 \quad \text{as} \quad F \to 0 \tag{50}$$

we can guarantee that the realizability conditions are satisfied.

4.5. *Effect of the Reynolds number*

In order to complete the present turbulence model, we must model the rate of return to isotropy as a function of the Reynolds number and the type and degree of anisotropy of turbulence, while satisfying the realizability conditions. Here we propose the following expression for ρ^*:

$$\rho^* = C_3 \exp\left(-\frac{C_1}{\sqrt{R_l}} - \frac{C_4}{R_1}\right)\left[\left\{1 - \exp\left(-\frac{(1-F)}{0.35}\right)\right\} g(X) + \frac{C_2}{\sqrt{R_l}}\right] \times \left[\frac{2}{1-3\Psi_s} - 1 - (1 + 0.717F^{2.66}R_l^{0.25})^{-2}\right]. \tag{51}$$

This expression is rather complicated; however all the terms in the equation are necessary to ensure that it will display the correct asymptotic behaviour for homogeneous turbulence as well as to agree with the experimental data. The basic form of equation (51) has been derived from the realizability argument in modelling the density anomaly flux (Lumley & Mansfield 1984), which is given by

$$\rho^* = 2\left\{1 - \exp\left(-\frac{(1-F)}{0.35}\right)\right\}\left[\frac{2}{1-3\Psi_s} - 1 - (1 + 0.75F^3\sqrt{R_l})^{-1}\right] \tag{52}$$

where

$$\Psi_s = \Psi + 2\Psi^2 + 7\Psi^3 + 30\Psi^4 + 143\Psi^5, \quad \Psi = \frac{4F}{27}. \tag{53}$$

Although this expression fits many of the experimental data, it does not have the correct asymptotic behaviour. It also lacks a proper functional dependence on the Reynolds number and on the type of anisotropy of the turbulence. In order to improve the model (52), we first require the following asymptotic behaviour of the homogeneous turbulence:

$$\rho^* \to 0 \quad \text{as} \quad \sqrt{R_l} \to 0, \tag{54}$$

which means that there will be no return to isotropy in the final period of decay (Lumley 1978; Lumley & Newman 1977). The return to isotropy is basically due to the nonlinear interaction between fluctuating velocities and pressure so that homogeneous anisotropic turbulence does not return to isotropy at vanishing Reynolds number where turbulence ceases to exist. The next requirement is that the model must agree with a series of experimental results by Comte-Bellot & Corrsin (1966) for cigar-shaped turbulence with vanishing anisotropy, which gives

$$\rho^* \to 0 \quad \text{with} \quad \sqrt{R_l} \to \infty \tag{55}$$

and in particular

$$\rho^* = 0.609 \quad \text{with} \quad \sqrt{R_l} = 12. \tag{56}$$

The first exponential term $\exp(-C_1/\sqrt{R_l})$ and the last term in the first square bracket $C_2/\sqrt{R_l}$ in equation (51) fulfil these requirements. We must also require that the turbulence model should predict not only the turbulence with low to moderate Reynolds number observed in the laboratories, but also atmospheric turbulence with

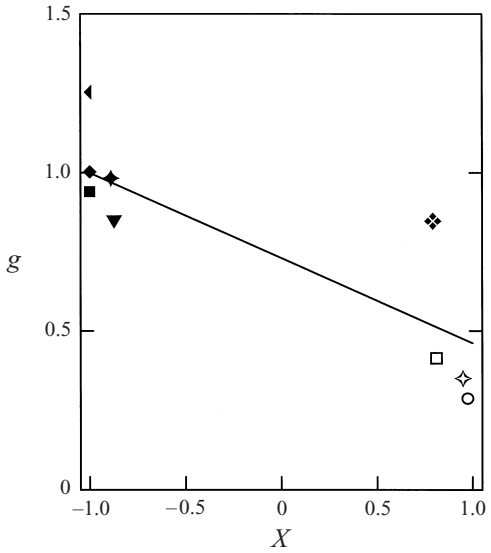

FIGURE 9. Function g vs. X to indicate the relative magnitude of the rate of return to isotropy of anisotropic turbulence to pancake-shaped turbulence. Symbols are as in figure 3.

$\sqrt{R_l} = O(10^3)$. In order for the turbulence model to cover such a wide range of Reynolds numbers, it is necessary to add one more exponential term $\exp(-C_4/R_l)$ to the expression for ρ^*. The numerical constants C_1, C_2, C_3 and C_4 in equation (51) are then determined to account for all the available experimental results after the axisymmetric contraction while satisfying the asymptotic behaviour of homogeneous turbulence as described above. The constants are given by $C_1 = 3.28$, $C_2 = 0.680$, $C_3 = 2.49$ and $C_4 = 8.69$.

Our experimental results at similar Reynolds numbers of $\sqrt{R_l} = O(10)$ indicated that the rate of return to isotropy is very different depending on the type of anisotropy of turbulence (figures 6 and 7). This can be demonstrated by plotting the function $g(X)$ versus X in figure 9, where $g = 1$ for pancake-shaped turbulence ($X = -1$). Here, the functional value of $g(X)$ indicates the relative magnitude of the rate of return to isotropy of homogeneous turbulence to pancake-shaped turbulence. Since no experimental data are available between $X = -0.8$ and 0.6, a straight line fit will give

$$g(X) = 1 - 0.269(X + 1). \tag{57}$$

Substituting (57) and all the numerical constants into (51) we finally obtain

$$\rho^* = 2.49 \exp\left(-\frac{3.28}{\sqrt{R_l}} - \frac{8.69}{R_l}\right)\left[\left\{1 - \exp\left(-\frac{(1-F)}{0.35}\right)\right\}\{(1 - 0.269(X+1)\} + \frac{0.680}{\sqrt{R_l}}\right] \times \left[\frac{2}{1 - 3\Psi_s} - 1 - (1 + 0.717F^{2.66}R_l^{0.25})^{-2}\right]. \tag{58}$$

Figure 10 shows the plot of the rate of return to isotropy ρ^* vs. F for all the experimental and numerical data for pancake-shaped axisymmetric turbulence ($X = -1$). The Reynolds number of all the data shown in the figure is $\sqrt{R_l} = O(10)$ except for the DNS data (Rogallo 1981) and for our data set 1 of the axisymmetric contraction experiment for which $\sqrt{R_l} = O(1)$. The predictions by the present turbulence model given by equation (58) are also shown in the same figure for a range of Reynolds

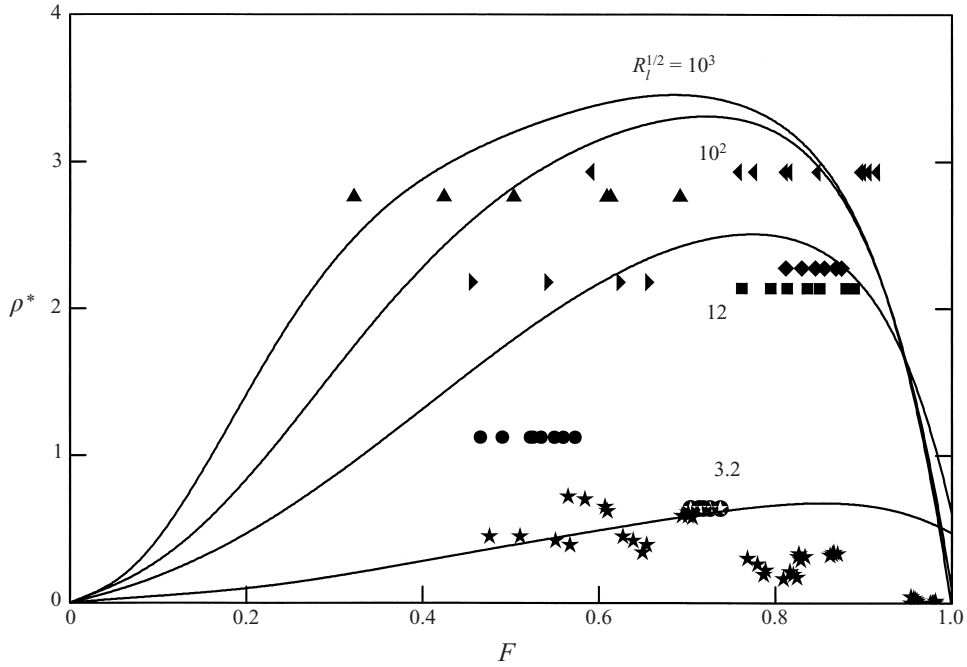

FIGURE 10. Predictions of the rate of return to isotropy of pancake-shaped turbulence ($X = -1$) by the present turbulence model for a range of the Reynolds numbers. Symbols are as in figures 3 and 6.

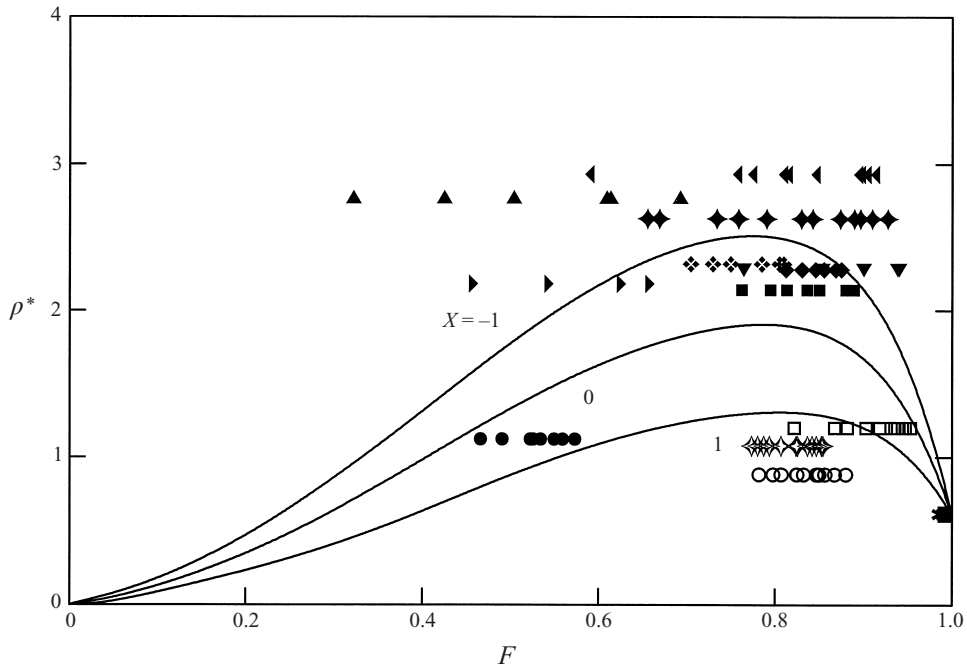

FIGURE 11. Predictions of the rate of return to isotropy of different types of anisotropic turbulence with $\sqrt{R_l} = 12$ by the present turbulence model. Symbols are as in figures 3 and 6.

numbers. The model predicts $\rho^* = 3.4$ at $F = 0.75$ when $\sqrt{R_l} = 10^3$, which is the right value for atmospheric turbulence. The agreement of the present model with Rogallo's DNS results is also good. The predictions of the rate of return to isotropy ρ^* for homogeneous turbulence with $\sqrt{R_l} = 12$ are plotted against F in figure 11 with X as the parameter. Remembering that $X = -1$ and $+1$ correspond to pancake-shaped and cigar-shaped turbulence, respectively the present turbulence model correctly predicts a faster return to isotropy for pancake-shaped turbulence and a slower return for cigar-shaped turbulence.

All the experiments and some of the data analysis were carried at Cornell University while the first author was a research assistant/post-doctoral associate. The rest of the analysis was carried out at British Maritime Technology, Teddington and at the University of Nottingham. The authors appreciate helpful comments provided by Professor S. B. Pope and fruitful discussions with Professor Z. Warhaft. They also thank Mr E. P. Jordan for his excellent technical assistance during the experiment. This research was supported in part by the US Office of Naval Research under the following programs: Physical Oceanography (Code 422PO), Fluid Dynamics (Code 438), Power (Code 473); in part by the US National Science Foundation under grant no ATM 79-22006 and CME 79-19817; and in part by the US Air Force Office of Scientific Research. The first author also acknowledges support from the Leverhulme Trust (RF&G/10988).

REFERENCES

Batchelor, G. K. & Proudman, I. 1954 The effect of rapid distortion of a fluid in turbulent motion. *Q. J. Mech. Appl. Maths* **7**, 83.

Bradshaw, P. 1975 *An Introduction to Turbulence and its Measurement*. Pergamon.

Bradshaw, P., Cebeci, T. & Whitelaw, J. H. 1981 *Engineering Calculation Methods for Turbulent Flow*. Academic.

Champagne, F. H., Harris, V. G. & Corrsin, S. 1970 Experiments on nearly homogeneous turbulent shear flow. *J. Fluid Mech.* **41**, 81.

Champagne, F. H., Sleicher, C. A. & Wehrmann, O. H. 1967 Turbulence measurements with inclined hot-wires, part 1: heat transfer experiments with inclined hot-wire. *J. Fluid Mech.* **28**, 153.

Choi, K.-S. 1983 A study of the return to isotropy of homogeneous turbulence. PhD thesis, Cornell University.

Choi, K.-S. & Lumley, J. L. 1983 Return to isotropy of homogeneous turbulence revisited. In *Turbulence and Chaotic Phenomena in Fluids* (ed. T. Tatsumi), pp. 267–272. North-Holland.

Chung, M. K. 1978 Study of second-order turbulence models with variable coefficients. PhD thesis, University of Illinois at Urbana-Champaign.

Comte-Bellot, G. & Corrsin, S. 1966 The use of a contraction to improve the isotropy of grid-generated turbulence. *J. Fluid Mech.* **25**, 657.

Gence, J. N. & Mathieu, J. 1980 The return to isotropy of an homogeneous turbulence having been submitted to two successive plane strains. *J. Fluid Mech.* **101**, 555.

Hanjalic, K. 1994 Advanced turbulence closure models: a view of current status and future prospects. *Intl J. Heat Fluid Flow* **15**, 178.

Hanjalic, K. & Launder, B. E. 1972 A Reynolds stress model of turbulence and its application to thin shear flows. *J. Fluid Mech.* **52**. 609.

Harris, V. G., Graham, J. A. & Corrsin, S. 1977 Further experiments in nearly homogeneous turbulent shear flows. *J. Fluid Mech.* **81**, 657.

Hwang, W. S. 1971 Experimental investigation of turbulent shear flows. PhD thesis, University of Virginia.

Ikai, K. & Kawamura, H. 1995 Direct simulation of homogeneous anisotropic turbulence by parallel computation. *Trans. JSME* B **61**, 868.

Jorgensen, F. E. 1971 Directional sensitivity of wire and fiber-film probes. *DISA Inf.* **11**, 31.

Kaminski, J. A. 1978 STAT; an interactive analog-to-digital sampling and time-series analysis program. Sibley School of Mechanical and Aerospace Engineering, Cornell University.

Kassinos, S. C. & Reynolds, W. C. 1997 Advances in structure-based turbulence modeling. *Annual Research Briefs*, pp. 179–193. Center for Turbulence Research.

Kinsler, L. E. & Frey, A. R. 1962 *Fundamentals of Acoustics*. John Wiley and Sons.

Launder, B. E. 1989 Second-moment closure: present ... and future? *Intl J. Heat Fluid Flow* **10**, 282.

Launder, B. E., Reece, G. J. & Rodi, W. 1975 Progress in the development of a Reynolds-stress turbulence closure. *J. Fluid Mech.* **68**, 537.

Lee, M. J. 1986 Numerical experiments on the structure of homogeneous turbulence. PhD thesis, Stanford University.

Lee, M. J. & Reynolds, W. C. 1985 On the structure of homogeneous turbulence. *Proc. 5th Symp. Turbulent Shear Flows, Cornell University*, pp. 17.7–17.12.

Le Penven, L., Gence, J. N. & Comte-Bellot, G. 1985 On the approach to isotropy of homogeneous turbulence: Effect of partition of kinetic energy among the velocity components. In *Frontiers in Fluid Mechanics* (ed. S. H. Davis & J. L. Lumley), pp. 1–21. Springer.

Lumley, J. L. 1970 *Stochastic Tools in Turbulence*. Academic.

Lumley, J. L. 1978 Computational modelling of turbulent flows. In *Advances in Applied Mechanics*, vol. 18, pp. 123–175. Academic.

Lumley, J. L. 1982 Homogeneous flows. In *1980–81 AFOSR-HTTM-Stanford Conf. on Complex Turbulent Flows: Comparison of Computation and Experiment* (ed. S. J. Kline, B. J. Cantwell & J. H. Ferziger), Vol. II. Stanford University.

Lumley, J. L. & Mansfield, P. 1984 Second order modelling of turbulent transport in the surface layer. *Boundary-Layer Met.* **30**, 109.

Lumley, J. L. & Newman, G. R. 1977 The return to isotropy of homogeneous turbulence. *J. Fluid Mech.* **82**, 161.

Makita, H. & Minami, K. 1995 Decay process of three-dimensionally anisotropic turbulence. *Trans. JSME* B **61**, 26.

Mills, R. R. & Corrsin, S. 1959 Effect of contraction in turbulence and temperature fluctuations generated by a warm grid. *NASA Memo.* 5-5-59W.

Nishino, K., Samada, M., Kasuya, K. & Torii, K. 1996 Turbulence statistics in the stagnation region of an axisymmetric impinging jet flow. *Intl J. Heat Fluid Flow* **17**, 193.

Okibane, Y. 1979 Turbulence modelling in homogeneous flows: determination of the rapid terms, PhD thesis, Cornell University.

Perry, A. E. 1982 *Hot-wire Anemometry*. Oxford University Press.

Reynolds, W. C. 1976 Computation of turbulent flows. *Ann. Rev. Fluid Mech.* **8**, 183.

Reynolds, W. C. & Kassinos, S. C. 1995 One-point modelling of rapidly deformed homogeneous turbulence. *Proc. R. Soc. Lond.* A **451**, 87.

Rogallo, R. S. 1981 Numerical experiments in homogeneous turbulence. *NASA TM*-81315.

Rogers, M. M. & Moin, P. 1987 The structure of the vorticity field in homogeneous turbulent flows. *J. Fluid Mech.* **176**, 33.

Rotta, J. C. 1951 Statistische Theorie nichthomogener Turbulenz, 1. Mitteilung. *Z. Physik* **129**, 547.

Sarkar, S. & Speziale, C. G. 1990 A simple nonlinear model for the return to isotropy in turbulence. *Phys. Fluids* A **2**, 84.

Schumann, U. 1977 Realizability of Reynolds-stress turbulence models. *Phys. Fluids* **20**, 721.

Sirivat, A 1983 Experimental studies of homogeneous passive scalars in grid-generated turbulence. PhD thesis, Cornell University.

Speziale, C. G. 1991 Analytical methods for the development of Reynolds-stress closures in turbulence. *Ann. Rev. Fluid Mech.* **23**, 107.

Tennekes, H. & Lumley, J. L. 1972 *A First Course in Turbulence*. The MIT Press.

Tucker, H. J. 1970 The distortion of turbulence by irrotational strain. PhD thesis, McGill University.

Uberoi, M. S. 1956 Effect of wind-tunnel contraction on free-stream turbulence. *J. Aero. Sci.* **23**, 754.

Uberoi, M. S. 1957 Equipartition of energy and local isotropy in turbulent flows. *J. Appl. Phys.* **28**, 1165.

WARHAFT, Z. 1980 An experimental study of the effect of uniform strain on thermal fluctuations in grid-generated turbulence. *J. Fluid Mech.* **99**, 545.

WYNGAARD, J. C. 1968 Measurement of small-scale turbulence structure with hot-wires. *J. Sci. Instrum.* **1**, 1105.

YAMAMOTO, K. 1985 Numerical simulation of the return to isotropy of homogeneous turbulence. *Tech. Rep.* TR-885. National Aerospace Laboratory, Japan.

ZEMAN, O. 1975 The dynamics of entrainment in the planetary boundary layer: a study in turbulence modelling and parameterization. PhD thesis, The Pennsylvania State University.